Selective Adsorption on Fluorinated Plastic Enables the Optical Detection of Molecular Pollutants in Water

R. Lanfranco,[1] F. Giavazzi,[1] M. Salina,[2] G. Tagliabue,[1] E. Di Nicolò,[3] T. Bellini,[1] and M. Buscaglia[1,*]

[1]*Dipartimento di Biotecnologie Mediche e Medicina Traslazionale, Università degli Studi di Milano, 20090 Segrate, Italy*

[2]*Proxentia S.r.l., 20135 Milano, Italy*

[3]*Solvay Specialty Polymers, 20021 Bollate, Milano, Italy*

(Received 27 November 2015; revised manuscript received 21 February 2016; published 18 May 2016)

Amorphous fluorinated plastic can be produced with a refractive index similar to that of water, a condition that makes it essentially invisible when immersed in aqueous solutions. Because of this property, even a small amount of adsorbed molecules on the plastic-water interface provides a detectable optical signal. We investigate two distinct substrates made of this material, characterized by different interface areas: a prism and a microporous membrane. We demonstrate that both substrates enable the label-free detection of molecular compounds in water even without any surface functionalization. The adsorption of molecules on the planar surface of the prism provides an increase of optical reflectivity, whereas the adsorption on the internal surface of the microporous membrane yields an increase of scattered light. Despite the different mechanisms, we find a similar optical response upon adsorption. We confirm this result by a theoretical model accounting for both reflection and scattering. We investigate the spontaneous adsorption process for different kinds of molecules: surfactants with different charges, a protein (lysozyme), and a constituent of gasoline (hexane). The measured equilibrium and kinetic constants for adsorption differ by orders of magnitudes among the different classes of molecules. By suitable analytical models, accounting for the effects of mass limitation and transport, we find a simple and general scaling of the adsorption parameters with the molecular size.

DOI: 10.1103/PhysRevApplied.5.054012

I. INTRODUCTION

The widespread availability of autonomous analytical devices enabling the real-time monitoring of a large number of sensible environmental parameters represents a futuristic scenario that is largely desirable but still far from practical realization. Over the past decades, a large effort has been devoted to the development of innovative molecular sensors, and many promising technical solutions have been delivered [1,2]. However, very few of these have been brought out of the laboratory and exploited in the realization of devices capable of sustaining the harsh conditions of the sites for environmental monitoring. The requirements for deployable autonomous systems include operational simplicity of the measurement, limited instrumental complexity, minimum cost of the device, high reusability, and resistance to chemical, biological, and physical stresses. These features are not easily combined in a single device that also must provide high detection performance. In the context of analytical laboratories, where the conditions are more favorable, colorimetric methods, infrared spectroscopy [3], liquid chromatography, and mass spectroscopy [4,5] are widely employed approaches to detect contaminants in liquids and solubilized media. However, the most common and widespread techniques to detect surfactants or oily compounds in water require the collection of suitable amounts of samples and preparation steps performed by highly specialized personnel in furnished laboratories [6]. Therefore, these techniques are typically expensive and time consuming. Innovative nanostructured materials [7], electrochemical transducers [8], and engineered biomolecular probes [9] may also provide improved detection performance in the controlled lab conditions. Nevertheless, all these approaches have so far failed to match all the requirements for an inexpensive deployable system.

Recent works show how the peculiar optical properties of certain amorphous perfluorinated polymer materials can be exploited to realize sensitive label-free biosensors based on simple components and requiring minimum sample processing [10,11]. In particular, amorphous copolymers of tetrafluoroethylene can be realized in order to present high transparency and a refractive index very close to that of water [12]. These materials become barely visible when immersed into an aqueous solution. Various surface treatments were developed to immobilize specific bioreceptors on their surface. This enables the detection of the binding of different biomolecular targets through the increase of the light scattered by suspended nanoparticles [13–15] or

*Corresponding author.
marco.buscaglia@unimi.it

reflected by the surface of a prism [10,16]. Despite the high performance for biomolecular detection, these systems present a few drawbacks that limit their exploitation in autonomous deployable platforms for on-line monitoring applications. In particular, the suspension of nanoparticles provides the advantage of a large sensing surface that facilitates the detection of small molecules in abundant sample volumes. However, the particles can form aggregates that complicate the analysis of the light-scattering signal. Additionally, the suspension format is not suitable for continuous use in fluidic circuits. In contrast, the planar reflective surface of the prism provides an ideal support for fluidic integration. However, in previous studies, the surface immobilization of specific biomolecular probes was required to provide the binding and therefore the detection. Consequently, the flexibility of measuring conditions, the reusability, and the storage of the sensing substrates are generally limited by the necessity to preserve the full functionality of the biomolecular recognition elements.

On the other hand, the index-matched perfluorinated substrates, when used as optical sensing materials, provide peculiar and interesting features, still largely unexplored: (i) Their surface in an aqueous environment is at the same time hydrophobic and negatively charged and induces the spontaneous adsorption of various molecular compounds; (ii) they exhibit a high resistance to chemical and biological stresses, and, therefore, they can be easily cleaned and regenerated [17,18]; (iii) substrates with different shapes and structures down to the micron scale can be easily realized by using conventional fabrication processes for plastic materials [19]. In principle, the spontaneous adsorption of different molecular compounds mentioned in (i) can be exploited to detect contaminants in aqueous solutions. However, the possible selectivity of the adsorption process onto index-matched perfluorinated plastics is largely undetermined. Previous studies on the electrokinetic properties of rodlike colloids made of crystalline polytetrafluoroethylene address the characterization of surfactant adsorption to control the surface charge of the particles [20,21]. More generally, the formation of an adsorbed molecular layer at the solid-liquid interface may represent a complex process, potentially involving various morphological rearrangements and different time scales [22–30]. Kinetics measurements are increasingly used to gain a deeper understanding of these phenomena [23]. Nevertheless, simple theoretical models suitable to predict the behavior of different classes of molecules are not yet available. In the case of surfactants, most studies focus on the adsorption behavior at relatively high concentrations across the critical micelle concentration (CMC). In contrast, in order to design sensitive detection systems, a suitable characterization and a modeling of the adsorption process at the lowest detectable concentrations are required.

Here we present a concept of optical-detection systems based on perfluorinated materials isorefractive with water. We realize a right-angle prism suitable for reflection measurements and a microporous membrane for light-scattering measurements. The presence of surfactants in solution yields an increase of the intensity of light reflected by the prism or scattered by the membrane due to the adsorption on their surface. We characterize the adsorption process at equilibrium for both systems. Remarkably, a common optical model accounts for both the reflection from the prism and the light scattered from the membrane upon adsorption of molecules. Through this model, the optical signals are converted into the thickness of the molecular layer formed at the interface, which is found to be in agreement with the size of the molecules. We obtain a detailed description and characterization of the adsorption process for different molecules by means of the prism system. Surfactants with different net charge, hexane, and the protein lysozyme spontaneously adsorb, providing different signals. Remarkably, both the equilibrium constants for adsorption and the kinetic parameters differ by orders of magnitude among the three classes of molecules. Overall, simple adsorption and transport models enable the identification of structural features related to the molecular size as important parameters affecting the adsorption process. These results indicate the possibility of different adsorption fingerprints enabling discrimination among different molecular compounds in aqueous samples and, therefore, provide the basis for a class of sensing materials, potentially suitable for on-line detection instruments with very low complexity.

The following sections are organized in this way: In Sec. II, we introduce the prism and membrane sensing substrates and propose a common optical model accounting for their signal upon adsorption. In Sec. III, we compare the response to different concentrations of surfactant for the two systems by a simple adsorption model. In Sec. IV, we compare the adsorption at equilibrium for different classes of molecules on the prism sensor and discuss the observed dependence of the adsorption strength on the molecular size. In Sec. V, the adsorption kinetics observed for the different molecules are interpreted considering diffusion and transport effects, which also scale with the molecular size. Section VI reports a summary of the main results.

II. OPTICAL SIGNAL FROM REFLECTANCE AND SCATTERING MEASUREMENTS

In this section, we describe two different sensing substrates index-matched with water: a prism and a microporous membrane. The adsorption of molecules at their interface yields an increase of reflected or scattered light intensity, respectively. For both systems, the signal increase is ascribed to the formation of a thin layer of different refractive index separating the solid and liquid media with similar refractive indices. We show that, in this index-matching condition and for a thickness h of the adsorbed layer much smaller than the wavelength of light λ, the reflected or scattered intensity I is related to the amount of adsorbed molecules by simple optical models. More

generally, other well-established techniques enable the characterization of the structure of a thin molecular layer on a planar surface by a detailed modeling of the spectrum and polarization of the reflected light [31,32]. In this work, we exploit a different approach: We simply measure the increase of the reflected or scattered intensity of monochromatic light upon the formation of the layer. We describe the quantity of adsorbed molecules through an effective thickness h that represents the thickness of an ideal homogenous layer with fixed refractive index n_l. For each compound, the value of n_l corresponds to the refractive index of a compact molecular layer, and the extracted thickness h is proportional to the amount of adsorbed molecules. By this simplified model, we derive a scaling of either the reflected or scattered intensity with h^2. The general formula to account for the intensity signal I in the presence of the adsorbed layer relative to the intensity I_0 measured in the absence of the layer is given by

$$\frac{I}{I_0} = 1 + \left(\frac{h}{h^*}\right)^2, \tag{1}$$

where the value of the parameter h^* corresponds to the layer thickness yielding to $I = 2I_0$ and, therefore, $1/h^*$ represents the sensitivity of the optical response to molecular adsorption. Knowing the value of h^*, Eq. (1) enables the conversion of the relative increase of reflected or scattered light intensity I/I_0 into the effective thickness h of the adsorbed molecular layer. Remarkably, we show that, despite the different optical mechanism and the different area of the adsorbing interface, the values of h^* for the prism sensor and for the microporous membrane are substantially identical.

A. Prism sensor

Mechanical machining, printing, and molding are common approaches for plastic manufacturing, which also apply to perfluorinated polymers. Prisms of Hyflon® AD (Solvay Specialty Polymers, Bollate, Italy) were previously produced by cutting and polishing and exploited for optical biosensing applications [10]. In this study, we use a similar prism without any surface coating or functionalization in order to detect and quantify the spontaneous adsorption of molecules on its planar surface. The prism is inserted in a 1-cm cuvette as show in Fig. 1(a). When immersed in water, the prism becomes barely visible. The adsorption of molecules with a refractive index different from that of water provides a clear increase of reflected light intensity that is measured by a simple optical setup, composed by a He-Ne laser and a photodiode. The cuvette hosting the prism also contains a stir bar, which provides the rapid mixing of the solution.

Amphiphilic compounds represent a suitable class of molecules to test the optical response to adsorption. Figure 2(a) reports the intensity of reflected light measured after the addition in a solution of increasing concentrations of the cationic surfactant benzyldimethylstearylammonium chloride monohydrate (SBSAC). The data refer to the equilibrium value of reflectivity measured about 500 s after the addition. A continuous increase of reflectivity is observed until a saturation is reached at a high concentration, corresponding to the full coverage of the prism surface.

From the Fresnel formulas for thin-film reflection [33], the measured value of reflectivity can be related to the thickness h of the layer formed by the adsorbed material [10]. For values of h up to dozens of nanometers, the reflected intensity I_R scales with h^2 in agreement with

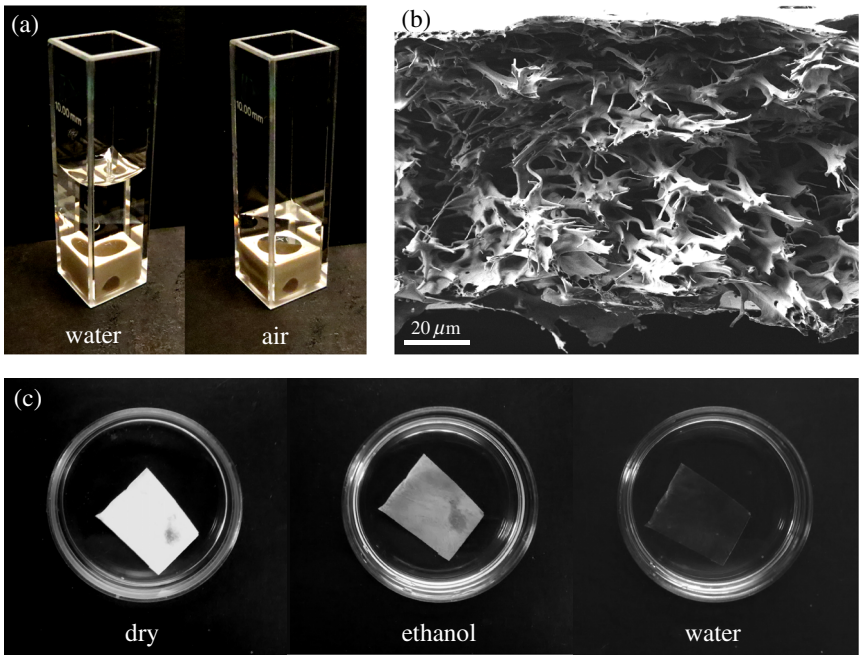

FIG. 1. Perfluorinated materials isorefractive with water. (a) Images of a prism of Hyflon® AD immersed in water and in air, as indicated. (b) Electron microscope image (SEM) of the cross section of the membrane of Hyflon® AD. (c) Images of the same membrane immersed in water or ethanol and in air, as indicated.

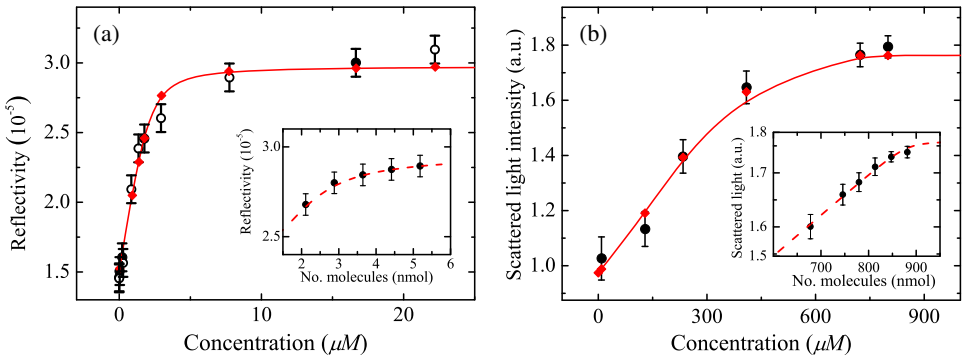

FIG. 2. Adsorption of a surfactant on different perfluorinated substrates index-matched to water. (a) Intensity of light reflected by the surface of the prism of Hyflon® AD for different concentrations of SBSAC in deionized water. At each addition, the sample volume in the cuvette is increased by 100 μl. Solid and open dots refer to data from different experiments. Diamonds represent the value extracted from the fit as a function of C_0 and V. The line is a spline to guide the eye. Inset: Reflected intensity as a function of the sample volume for a constant concentration of 1.92 μM (dots) and fitting curve (dashed line). (b) Intensity of light scattered by the microporous membrane of Hyflon® AD for different concentrations of SBSAC in deionized water. Dots and diamonds refer to experimental data and fitting value, respectively. The line is a spline to guide the eye. Inset: Scattered light intensity as a function of the quantity of molecules in the cuvette for a constant concentration of 340 μM (dots) and fitting curve (dashed line).

Eq. (1), where $I = I_R$, and I_0 represents the intensity reflected by the bare surface. For small differences between the refractive indices of the solution and the solid material, n_s and n_m, respectively, the value of h^* is given by

$$h^* = \frac{\lambda}{4\pi}\frac{\delta}{\bar{n}(\Delta - \frac{\delta}{2})}\left(1 - \frac{\Delta}{2\bar{n}}\right)\cos(\theta_i)^{-1}, \qquad (2)$$

where $\bar{n} = (n_s + n_m)/2$, $\delta = |n_s - n_m|$, $\Delta = n_l - \bar{n}$, n_l is the refractive index of the adsorbing layer, and θ_i is the angle of incidence relative to the surface normal. Compounds with different refractive index n_l yield to different values of h^* according to Eq. (2). For the materials and the geometry exploited in this study and in the case of adsorption of SBSAC on the prism surface, $h^* = 3.1$ nm. Consequently, the saturation value of reflectivity at a high concentration reported in Fig. 2(a) corresponds to a thickness $h_{\max}$ of about 3 nm, in agreement with the molecular size of the surfactant, as further discussed below.

B. Microporous membrane

Specifically designed methods are typically required to produce substrates with three-dimensional microstructures, such as micron-size pores [34]. Here we report the realization of a microporous membrane made by Hyflon® AD, the same perfluorinated material used for the prism. The membrane is produced by nonsolvent-induced phase separation, as described in Appendix A. In the context of small-molecule detection, as in the case of environmental-monitoring applications, flow-through systems with a high internal surface are expected to enhance the detection signal and the capture efficiency. A SEM image of a membrane with a thickness of about 100 μm is reported in Fig. 1(b). The internal structure is qualitatively similar to that of commercially available membrane filters realized with more conventional materials [35,36]. Interconnected pores with the size of a few microns are present. The macroscopic optical appearance of the membrane strongly depends on the refractive index of the liquid filling the pores. As shown in Fig. 1(c), the membrane appears white when completely dried, rather opaque when soaked with ethanol, and transparent in water. The measured turbidity of the membrane in water is as low as 1.2 mm^{-1}, meaning that more than 90% of the incident photons are not affected by scattering.

Figure 2(b) reports the scattered light intensity measured at an angle of 30° while illuminating the perfluorinated membrane with a diode laser at 532 nm (Coherent Compass 315M-100). The membrane is mounted on a rigid frame and immersed into a 1-cm cuvette. The mixing of the solution is provided by a magnetic stirring bar. The scattering signal increases rapidly after the addition of the surfactant SBSAC to the water solution and reaches an equilibrium value in a few seconds. Figure 2(b) reports such equilibrium values measured about 500 s after the addition. The scattered light intensity increases as a function of the surfactant concentration until reaching a plateau corresponding to the full coverage of the membrane surface.

C. Optical signal from the microporous membrane

We estimate the dependence of the light-scattering signal on molecular adsorption by a simple model. We consider the intensity of scattered light for a collection of independent spherical particles with radius R and with refractive index n_m close to that of the surrounding solution, n_s. In general, the same calculation can be extended to particles of any shape characterized by some effective size $2R$. We consider the theoretical framework of the Rayleigh-Gans (RG) approximation [37], whose validity for nearly

index-matching conditions extends to rather large values of R. Following the approach described in Ref. [38], we compute the intensity I_s of light scattered by the particles coated with a thin layer with refractive index n_l and thickness $h \ll R$. In the limit of small values of the thickness h, we obtain

$$I_s = C\left\{(n_m{}^2 - n_s{}^2)\mathcal{F} + (n_l{}^2 - n_s{}^2)\frac{d\mathcal{F}}{dR}h\right\}^2, \quad (3)$$

where C is a constant that depends on the number of particles and on the experimental setup. The function $\mathcal{F}$ is given by

$$\mathcal{F} = \int_V e^{i\boldsymbol{k}\cdot\boldsymbol{r}}dV, \quad (4)$$

where V is the particle volume, $\boldsymbol{k}$ is the scattering vector, and $\boldsymbol{r}$ is the vector indicating the position in space of the volume dV. In the limit of small particles ($kR \ll 1$), $\mathcal{F} = V$ up to a phase factor, and the behavior previously observed for nanoparticles isorefractive to water is recovered [13]. In this case, the light-scattering increment I_s/I_0 relative to the intensity I_0 scattered by the bare particles is also described by Eq. (1) with $I = I_s$, assuming an even distribution of solid particles in the solution and solution droplets embedded in the solid matrix, in order to account for the presence of convex and concave surface regions, respectively. Accordingly, for small spherical particles, the value of the parameter h^* is given by

$$h^* = \left|\frac{n_m{}^2 - n_s{}^2}{n_l{}^2 - n_s{}^2}\right|\frac{R}{3}. \quad (5)$$

As expected, smaller particles provide a higher relative increment of scattered light due to the coating layer, and the sensitivity scales linearly with $1/R$ [13].

A different scenario is expected for large particles ($kR \gg 1$). However, a unifying model enabling the comparison of the optical response of a scattering system with that of the reflective surface is missing. Remarkably, we find that the simple RG framework is suitable to perform this evaluation. We consider a system of large particles and compute the average intensity of scattered light over a distribution of R with width ΔR. We assume a polydispersity of sizes such that $k\Delta R \gg 1$. This enables the neglect of the linear term $\langle\mathcal{F}(d\mathcal{F}/dR)\rangle$ obtained from Eq. (3), because $d\mathcal{F}/dR$ and $\mathcal{F}$ are both oscillating quantities as a function of R and they are in quadrature of phase, so the mean value of their product is equal to zero. Accordingly, a dependence of I_s on h^2 is recovered, and the relative increment of scattered light due to the coating layer is given, in general, by

$$\frac{I_s}{I_0} = 1 + \left(\frac{n_l{}^2 - n_s{}^2}{n_m{}^2 - n_s{}^2}\right)^2 \frac{\left\langle\left(\frac{d\mathcal{F}}{dR}\right)^2\right\rangle}{\langle\mathcal{F}^2\rangle}h^2. \quad (6)$$

In the limit of large particles and large polydispersity, the ratio between the two averaged quantities is simply equal to the squared modulus of the scattering vector, k^2, as can be easily demonstrated in the case of spherical particles. The description provided by Eq. (1) holds also in the condition of large particles, and the corresponding value of h^* is given by a surprisingly simple equation:

$$h^* = \left|\frac{n_m{}^2 - n_s{}^2}{n_l{}^2 - n_s{}^2}\right|\frac{1}{k}, \quad (7)$$

where the modulus of the scattering vector is given by $k = 4\pi n_s \sin(\theta_s/2)/\lambda$ and θ_s is the angle formed between the scattered and incident rays. For the materials and the setup geometry employed in this study, in the case of adsorption of SBSAC on the membrane surface, $h^* = 3.4$ nm. Accordingly, the saturation value at a high concentration reported in Fig. 2(b) corresponds to a thickness $h_{\max}$ of about 2.7 nm. Remarkably, this value is very similar to that obtained with the prism sensor for the same surfactant.

D. Comparison of the optical response of reflective and scattering materials

The simplified models developed here enable the evaluation of the expected response of different materials isorefractive to water by comparing the values of h^*, as defined in Eqs. (2), (5), and (7). As anticipated, the scattering systems can ideally yield a higher sensitivity for a smaller size of the particles [Eq. (5)]. However, upon increasing the particle size, the parameter h^* reaches the value for large particles [Eq. (7)] when R is still significantly smaller than λ. By comparing Eqs. (5) and (7), in the case of backscattering ($\theta_s = 180°$), the value of h^* for large spherical particles is reached for $R = 3\lambda/(4\pi n_s)$, which, considering the parameters employed in this study, approximately corresponds to values as low as 100 nm.

In order to compare the sensitivity of the prism sensor and the membrane system, a common notation is needed to indicate the direction of the reflected or scattered ray. In the case of the reflective system, the angle of incidence θ_i relative to the surface normal can be written in terms of the scattering angle θ_s as $\theta_i = 90° - \theta_s/2$. Remarkably, the value of h^* defined in Eq. (7) is nearly identical to that of the reflective surface reported in Eq. (2), when a common angle θ_s is considered. Moreover, the dependence on n_l is also similar: In both equations, $1/h*$ roughly scales with $n_l - n_s$ with a small quadratic correction. Therefore, despite the different optical signals and surface areas, the detections based on prism reflectivity and membrane scattering are expected to present a similar dependence on the amount of adsorbing material, at least for membranes with large enough internal structures, as the one considered here [Fig. 1(b)]. Indeed, this is experimentally confirmed by the similar saturation values of I_R/I_0 and I_S/I_0 at high amounts of surfactants reported in Figs. 2(a) and 2(b), respectively. Moreover, as anticipated, considering the values of h^*, the obtained thickness $h_{\max}$ of the adsorbed molecular layer

is similar in the two cases, being about 3 nm for both systems.

III. CHARACTERIZATION OF MOLECULAR ADSORPTION

In the following, we introduce a simple adsorption model, which relates the optical response of the prism and membrane systems to the amount of adsorbing molecules added in solution. Here we consider the equilibrium behavior of adsorption. We show that the response of the membrane is primarily ascribed to the large interfacial area, whereas the adsorption on the prism sensor also depends on the strength of the interaction with the surface.

A. Adsorption model

As shown in Figs. 2(a) and 2(b), a saturation of the adsorption signal at a high concentration of surfactants is observed for both the prism and the membrane. However, the saturation intensity $I_{\max}$ is reached at much higher concentrations in the case of the membrane. This difference can be ascribed to the different area of the adsorbing interface, which is much larger in the case of the membrane. This also implies that, at least for the membrane, the dependence of the adsorption signal on the surfactant concentration is dominated by the limited amount of molecules relative to the available adsorption sites. To further investigate this hypothesis, we also perform experiments on SBSAC adsorption increasing the total amount of molecules in solution at a fixed concentration. As shown in the insets in Figs. 2(a) and 2(b), a signal increase and a saturation are observed also in these experiments, for both the prism and the membrane. This behavior indicates the presence of a large total area available for adsorption with a high affinity for the surfactant, as further discussed in the following.

The theoretical framework for the investigation of the adsorption process is provided by the Langmuir model, arguably the simplest adsorption model, which is based on the assumption of independent binding events onto the surface [39]. Remarkably, this approach is found to well represent the observed behavior despite the possible complexity involving the formation of an adsorbed molecular layer at the solid-liquid interface [23]. The agreement of the extracted value of $h_{\max}$ with the molecular size suggests the formation of a molecular monolayer on the surface. This enables the modeling of the adsorbing interface as a two-dimensional collection of binding sites and the addressing of the fraction of occupied sites $\varphi(C_0)$ as a function of the concentration C_0 of molecules added in the cuvette. The value of $\varphi(C_0)$ can be obtained from the thickness h of the adsorbed layer as $\varphi(C_0) = h(C_0)/h_{\max}$, which combined with Eq. (1) gives

$$\varphi(C_0) = \sqrt{\frac{I(C_0) - I_0}{I_{\max} - I_0}}. \tag{8}$$

Relevant parameters of the adsorption model are the kinetic constants for adsorption, k_{on}, and desorption, k_{off}, as well as their ratio $K_d = k_{\text{off}}/k_{\text{on}}$, which is the equilibrium constant for desorption. Another important parameter is represented by the total amount of binding sites N_s, which provides the maximum molar quantity of analyte molecules removed from the solution and adsorbed onto the available surface at saturation. In general, large enough values of N_s are expected to affect both the equilibrium and the kinetic parameters, since the concentration of analyte in the solution may decrease significantly during the adsorption process, yielding mass-limitation effects. In this frame, the concentration C of analyte available in the solution is given by

$$C = C_0 - \varphi N_S/V, \tag{9}$$

where V is the volume of the liquid phase and, thus, the term N_S/V represents the concentration of adsorption sites in the cuvette and $\varphi N_S/V$ represents the concentration of molecules adsorbed onto the available surface. Since the adsorption process is substantially governed by the concentration C of available analytes in the solution, according to Eq. (9), a similar signal could, in principle, be generated by changing either the concentration C_0 in the cuvette or the sample volume V at some fixed concentration. As anticipated, this behavior is indeed observed for the experimental conditions here employed, as shown in the insets in Figs. 2(a) and 2(b). Importantly, the prism setup enables the minimization of the mass-limitation effects through the accessibility of lower values of N_S/V relative to the membrane system. Nevertheless, the correction of Eq. (9) is considered for both materials to properly extract the adsorption parameters. According to the Langmuir model, and considering Eq. (9), the progress of φ with time after a change of C_0 or V is given by

$$\frac{d\varphi(t)}{dt} = k_{\text{on}}\left[C_0 - \frac{N_S}{V}\varphi(t)\right][1 - \varphi(t)] - k_{\text{off}}\varphi(t). \tag{10}$$

In the following, we address the equilibrium behavior of Eq. (10). The time-dependent behavior is discussed in Sec. V for different molecules.

B. Equilibrium response of the prism and membrane to the amount of adsorbing molecules

Solving Eq. (10) for $d\varphi/dt = 0$ provides the fraction of occupied binding sites at equilibrium, φ_{eq}, for a particular concentration C_0 and for a total amount of molecules C_0V. The analytical form of φ_{eq} is given by

$$\varphi_{\text{eq}} = \frac{V(C_0 + K_d) + N_s - \sqrt[2]{[V(C_0 + K_d) + N_s]^2 - 4VC_0N_s}}{2N_s}. \tag{11}$$

This equation enables the extraction of the concentration $C_{1/2}$ at which half of the binding sites are occupied:

$$C_{1/2} = K_d + \frac{1}{2}\frac{N_S}{V}. \quad (12)$$

According to Eq. (12), both parameters K_d and N_s must be considered in order to account for the experimental behavior of $\varphi_{eq}(C_0)$ [40]. The values of these parameters are obtained from the concomitant fit of the data of φ_{eq} as a function of C_0 and V by Eq. (11). Figures 2(a) and 2(b) and their insets report the curves fitting the data of reflected and scattered intensity, respectively. In the case of the prism sensor, the two sets of data enable the extraction of both parameters. The K_d obtained for SBSAC on the prism surface is 165 nM, and the corresponding amount of binding sites N_S is 2.17 nmol. In the case of the membrane, the value of K_d is assumed to be the same as the prism, and the value of N_S extracted from the fit is about 0.88 μmol, that corresponds to an available area for adsorption about 400 times larger than that of the prism surface. This value is consistent with the inner surface area obtained from flow-resistance measurements performed on commercially available membranes with similar characteristics [41]. Therefore, the membrane system requires a larger amount of surfactants to provide the same relative increase of optical signal observed with the prism, because of the larger adsorbing interface. Nevertheless, for applications where the amount of sample is not a relevant limitation, the membrane sensor can still provide practical advantages by enabling a unique combination of filtering and detection capabilities, which can facilitate the development of analytical systems for the on-line detection of adsorbing compounds.

IV. STRENGTH OF ADSORPTION FOR DIFFERENT MOLECULES

In this section, we compare the behavior of adsorption at equilibrium on the prism sensor for different classes of molecules. We repeat the analysis with the adsorption model introduced in the previous section on different surfactants, a protein, and a small hydrophobic molecule. We discuss the thickness of the adsorbing layer and the equilibrium constant for adsorption extracted for the different molecules. We show that the adsorption strength scales with the hydrophobic portion of the molecular contact area on the sensor surface.

A. Equilibrium constant for adsorption

The analysis reported above shows that the planar surface of the prism enables a more comprehensive characterization of the parameters affecting the spontaneous adsorption of molecules relative to the microporous membrane. Indeed, according to Eq. (12) and as confirmed by the experiments, in the case of the membrane the response to the surfactant concentration is ascribed to the large inner surface, whereas the adsorption on the smaller prism surface depends on the equilibrium constant. Moreover, as discussed in Sec. V below, the prism also facilitates the kinetic modeling of the molecular transport from the bulk solution onto the surface and vice versa. Therefore, we exploit the prism format to investigate the interaction between different kinds of molecules bearing hydrophobic moieties and the bare surface of the perfluorinated material used to fabricate both the prism and the membrane.

Molecular compounds with a refractive index as low as that of water are rare. Therefore, a very large variety of molecules could yield an optical signal upon adsorption on the prism sensor. In order to compare the adsorption of different classes of molecules, we study three surfactants, the protein lysozyme, and hexane, which is a paraffin that represents an important constituent of gasoline. The chosen surfactants have different net charges and molecular structures. In addition to the cationic surfactant SBSAC, we investigate the anionic sodium dodecyl sulfate (SDS) and the nonionic polysorbate 20 (Tween 20) (Sigma Aldrich). The physicochemical characteristics of these molecules are reported in Table I. The experiments are performed either in deionized water (MilliQ®) or by using a buffer composition resembling the salinity of river water (0.049 mM magnesium chloride, 0.09 mM calcium chloride, 1 mM phosphate buffer, 0.27 mM potassium chloride, and 13.7 mM sodium chloride). All the concentrations investigated in this study are well below the expected CMC of the surfactants (Table I).

Similarly to the study performed on SBSAC, the saturation values of h extracted about 500 s after the

TABLE I. Physical parameters of the studied molecules.

Molecule	MW[a] (Da)	CMC[b] (mM)	ρ[1] (g/ml)	n[c]	D[c] (10^{-6} cm^2/s)	h^* (nm)
SBSAC deion. water	442.15	0.34	0.376	1.435	4	3.2
SBSAC buffer		0.13				
Tween 20	1227.54	0.30	1.1	1.469	1	2.4
SDS	288.37	0.54	1.01	1.461	1.76	2.5
Lysozyme	14000		1.2	1.5	1.10	1.9
Hexane	86.18		0.655	1.373	2.3	8.4

[a]Molecular mass and density are taken from the data sheets of the compounds or from Ref. [42] in the case of lysozyme.
[b]CMC is obtained by electrical conductivity measurements.
[c]Refractive indices and diffusion coefficients are taken from Refs. [43–46].

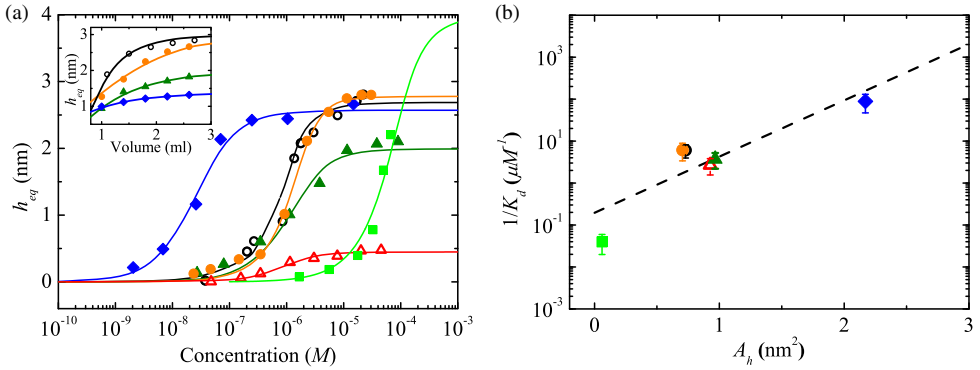

FIG. 3. Equilibrium of molecular adsorption on the prism surface. The thickness of the adsorbed layer at equilibrium h_{eq} is reported for different concentrations of SBSAC in deionized water (black open circles) and in a saline buffer (orange solid circles) and for Tween20 (green solid triangles), SDS (red open triangles), lysozyme (blue solid diamonds), and hexane (light green squares) in a saline buffer. At each addition, the sample volume in the cuvette is increased by 50–200 μl. The lines with corresponding colors represent the fits with the Langmuir adsorption model with a mass limitation. Inset: h_{eq} measured as a function of the sample volume at a fixed concentration (SBSAC in deionized water, 1.92 μM; SBSAC in a saline buffer, 1.08 μM; Tween 20, 1.62 μM; lysozyme, 19.3 nM). The color code is the same as in the main panel. (b) Value of the equilibrium adsorption constant $1/K_d$ extracted for each molecule from the fit of the data in (a) as a function of the hydrophobic molecular contact area A_h on the perfluorinated surface. The color code is the same as in (a). The black line represents a fit to the data with the function $\log_{10}(1/K_d) = C_1 + C_2 A_h$, where $C_1 = 5.29(\pm 0.42)$ and $C_2 = 1.34(\pm 0.37)$ nm^{-2}.

addition of the analyte in a cuvette provide a measurement of the equilibrium thickness of the adsorbed layer h_{eq}, reached for a particular concentration C_0 and for a total amount of molecules $C_0 V$. Figure 3(a) and its inset report the values of $h_{eq}(C_0, V)$ for the different molecules considered. By increasing the concentration C_0 or the volume V at a fixed concentration, a saturation of the adsorption is generally observed. Remarkably, the different classes of molecules display very different behaviors. The protein lysozyme displays a response at concentrations much smaller than surfactants, whereas hexane provides a detectable signal at much higher concentrations.

For each molecule, the adsorption curves as a function of C_0 and V are concomitantly fitted by using Eq. (11), and the parameters K_d, N_s, and h_{max} are obtained. The results are reported in Table II. In particular, the obtained K_d values are in agreement with the typical equilibrium constants reported for similar surfactants adsorbing on solid surfaces [47]. The behaviors of the cationic and nonionic surfactants are very similar. Surprisingly, also the anionic surfactant in saline buffer presents values of K_d and N_s similar to the other surfactants, despite the lower thickness h_{max} at saturation. These results suggest that the intrinsic affinity of surfactants for the perfluorinated surface does not depend directly on the net charge of the hydrophilic head, at least in a saline buffer. Additionally, the results indicate that, in general, different molecular structures can yield a very similar interaction with the surface. On the other hand, lysozyme and hexane display very different affinities and numbers of binding sites on the surface: The values of K_d and N_s are orders of magnitude different from those of surfactants. In particular, the protein has a higher affinity (lower value of K_d) and fewer binding sites, whereas hexane had a lower affinity and many more adsorption sites. In all cases, it is found that $N_s/V > K_d$, hence confirming that the adsorption process is affected by mass limitation.

B. Thickness of the adsorbed molecular layer

The different molecular classes here investigated show different increments of reflected intensity at saturation I_{max}/I_0, as reported in Table II. Remarkably, similarly to

TABLE II. Adsorption parameters obtained from the analysis.

Molecule	I_{max}/I_0	h_{mol}[a] (nm)	h_{max} (nm)	A_{mol} (nm^2)	K_d (nM)	N_S (nmol)	k_{on} (10^3 M^{-1} s^{-1})	k_{off} (10^{-3} s^{-1})
SBSAC deion. water	1.72	2.41	2.7	0.73	165	2.17	4.43	0.70
SBSAC buffer	1.77		2.8	0.70	163	2.79	3.51	0.57
Tween 20	1.72	2.0	2.00	0.93	372	2.33	1.86	0.69
SDS	1.03	1.77	0.45	0.97	270	1.33	8.5	2.3
Lysozyme	2.85	2.93	2.6	7.8	11.3	3.08×10^{-2}	107	1.21
Hexane	1.22	0.78	4.0	0.06	≥25200	185	≤0.013	0.33

[a]Molecular height is estimated by molecular modeling using ChemBioDraw 3D.

SBSAC, for all the studied surfactants and the protein, the corresponding values of h_{max} are in agreement with the sizes of the molecules (Table II) estimated by molecular modeling [48]. This indicates the formation of a molecular monolayer at the perfluoropolymer-water interface. For surfactants, the thickness of the adsorption layer also indicates a rather oriented structure of the amphiphilic molecules, which substantially stand on the surface, facing the hydrophobic group toward the plastic material. This interpretation is coherent to other experimental observations of surfactant adsorption on hydrophobic surfaces made by different techniques for concentrations below the CMC [49,50]. The anionic SDS represents an exception, because the value of h_{max} lower than the molecular size indicates a lower degree of packing relative to the other surfactants. The observed behavior of hexane is different from those of the other molecules: The maximum thickness extrapolated at high concentrations is not compatible with a single molecular layer. In this case, the process could be more rigorously described by a multilayer adsorption model [51]. Therefore, for hexane the value of K_d extracted with the Langmuir model represents an upper limit, and the thickness of the corresponding monolayer of hexane is derived from the expected geometric packing (Table II).

C. Scaling of the adsorption strength with the molecular contact area

A useful parameter to interpret the different values of adsorption affinities is represented by the contact area per molecule A_{mol} on the surface. In general, stronger interactions are expected for higher numbers of surface-interacting sites per molecule. For instance, it is observed that larger proteins tend to stick to various kinds of surfaces, whereas smaller ones adsorb only on interfaces with lower wettability [52]. For the studied molecules, the values of A_{mol} is obtained as $A_{mol} = V_{mol}/h_{max}$, where V_{mol} is the molecular volume estimated either as the molecular mass divided by the density or from the molecular structure. Remarkably, despite the different net charge and geometry, the obtained contact area is similar for all the considered surfactants, being in the range 0.7–1.0 nm^2. This result is in agreement with the maximum packing obtained from geometrical constraints that is estimated to be in the range 0.8–1.2 nm^2. As expected, the surface contact areas for lysozyme and hexane are very different from those of surfactants. A value of 7.75 nm^2 is obtained from the adsorption of the protein. This is consistent with the expected packing of the folded molecule onto the surface. Differently, the average contact area per hexane molecule is found to be 0.06 nm^2, significantly smaller than the estimated geometrical packing of 0.31 nm^2, in agreement with the hypothesis of the formation of a molecular multilayer onto the surface, as also derived from the analysis of the thickness of the adsorbed layer.

The experimental observations indicate that the equilibrium constant for adsorption on the perfluorinated surface does not depend on the net charge of surfactants and depends instead on the class of the molecule (i.e., paraffin versus surfactant versus protein). On the basis of these results, we test the consistency of a simple model for molecular adsorption on the perfluorinated surface. We assume that only the hydrophobic moieties of the molecules adhere to the surface and that all the hydrophobic interactions have the same strength per unit surface. With these assumptions, a linear scaling of the binding free energy with the hydrophobic portion A_h of the molecular contact area A_{mol} is expected. In the case of hexane and all the surfactants, the measured contact area A_{mol} is all ascribed to hydrophobic moieties; therefore, $A_h = A_{mol}$. Differently, only a fraction of the amino acids composing the protein lysozyme can be considered hydrophobic. Accordingly, in this case we assume $A_h = f_h A_{mol}$, where $f_h = 0.28$ is obtained as the fraction of hydrophobic residues (W, F, Y, L, I, C, M) over the entire protein sequence [53]. Figure 3(b) reports the measured value of the equilibrium constant for adsorption $1/K_d$ as a function of A_h. Remarkably, despite the diversity of the molecules, a scaling of $\log(1/K_d)$ with A_h is observed. From this dependence, we derive a free-energy increment for molecular adsorption of about -1.83 kcal mol^{-1} nm^{-2}. This value is in agreement with the adsorption free energy per hydrocarbon unit reported in previous works, which typically is in the range 0.2–0.6 kcal mol^{-1} [47,54,55]. Moreover, the estimated adsorption strength is coherent with the reported free energy of hydrophobic interactions among amino acids [53]. Overall, these observations are in agreement with the hypothesis of a relevant contribution of the hydrophobic contact area to the adsorption free energy on the perfluorinated surface and suggest the validity of this approach to predict the surface-binding affinity from the molecular size and structure.

V. KINETICS OF TRANSPORT AND ADSORPTION

In this section, we report the measured adsorption kinetics for the different molecular compounds addressed in the previous section. We analyze the data by using the time-dependent Langmuir model for adsorption introduced in Sec. III, which accounts for mass-limitation effects. Additionally, we consider the effect of transport limitation on the observed kinetics and propose a suitable model, which relates the adsorption kinetics to a transport parameter that ultimately depends on the molecular size.

A. Observed adsorption kinetics

The label-free detection based on the prism setup also enables direct access to the adsorption kinetics. The adsorption formula reported in Eq. (10) provides the time behavior of $\varphi(t)$. The general analytic form of $\varphi(t)$ is a

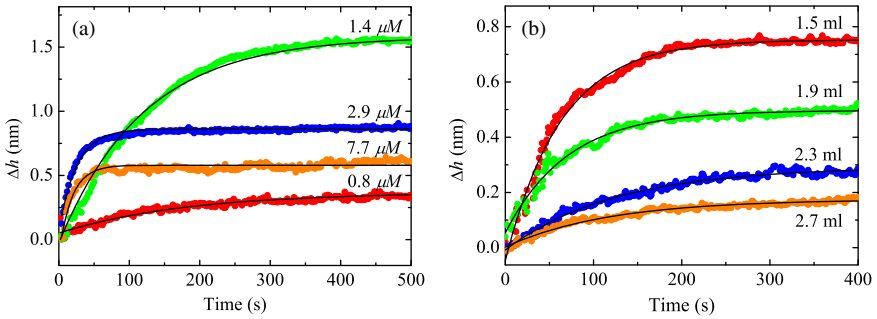

FIG. 4. Adsorption curves measured with the prism sensor. (a) Increment of the adsorbed layer thickness Δh as a function of time after the addition of increasing concentrations of SBSAC in deionized water, starting from 0.27 μM. The black lines represent exponential fitting curves. (b) Adsorption curves Δh of SBSAC in deionized water and exponential fits (black lines) obtained for increasing sample volumes, starting from 1.1 ml, at fixed concentration $C_0 = 1.92\ \mu M$.

hyperbolic tangent, which, in practice, differs only slightly from a single exponential behavior for all the conditions of interest in this study. This is because the coefficient of the term linear in φ is always larger than that of the quadratic one. Therefore, fitting the experimental adsorption curves with single exponential functions practically represents a good approximation and provides a robust approach to extract the kinetics parameter of the process.

Figure 4(a) reports the thickness increment $\Delta h(t) = h(t) - h(0)$ measured on the prism after a change of the SBSAC concentration in the cuvette at $t = 0$. The adsorption of SBSAC reaches an equilibrium within a few minutes after the addition of the surfactant. The observed kinetics become faster at higher concentrations. The growth Δh is well fitted by single exponential curves, as expected. Notably, also the adsorption curves measured after a change of volume are well fitted by single exponential functions, as shown in Fig. 4(b).

We extract the characteristic rate for adsorption $\Gamma(C_0, V)$ for the different molecular compounds considered in Sec. IV. The rates measured as a function of the concentration C_0 are plotted in Fig. 5(a). Generally, the rate increases with the concentration of analyte, in agreement with the Langmuir model of Eq. (10). The data points can be grouped in three classes corresponding to the three kinds of molecules. All surfactants have rather similar kinetics, coherently with the results obtained from the equilibrium analysis. The protein also shows a behavior at low concentrations similar to that of surfactants, whereas the kinetics at high concentrations become much faster. On the contrary, the hexane data indicate a much slower adsorption kinetics. In general, the observed rates are in agreement with other studies on the kinetic of surfactant adsorption performed below the CMC [50,56]. The inset in Fig. 5(a) reports the rates as a function of the sample volume in a cuvette at constant concentration. In agreement with Eq. (10), the observed decrease of $\Gamma(V)$ is ascribed to the effect of mass limitation, as further discussed below.

B. Kinetic model for adsorption

In order to compare the measured adsorption rates with those predicted by the model, we calculate effective adsorption rates from Eq. (10). We consider the initial, linear growth of adsorption after a concentration or volume increase. In the case of an exponential growth with amplitude φ_{eq} and rate Γ, the initial slope is given by

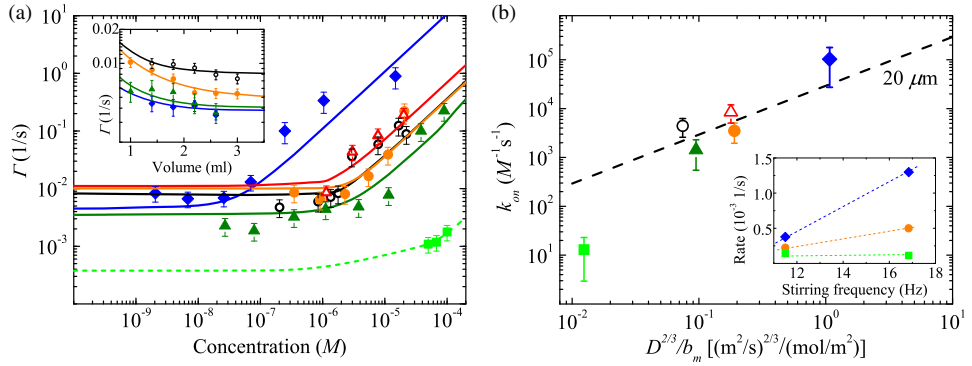

FIG. 5. Kinetics of molecular adsorption on the perfluorinated surface. The rates Γ extracted from the exponential fit of the adsorption curves are reported as a function of the concentration of SBSAC in deionized water (black open circles) and in saline buffer (orange solid circles) and for Tween20 (green solid triangles), SDS (red open triangles), lysozyme (blue solid diamonds), and hexane (light green squares) in a saline buffer. The lines with the corresponding color represent linear fits. Inset: Γ measured as a function of the sample volume at fixed concentration (SBSAC in deionized water, 1.92 μM; SBSAC in a saline buffer, 1.08 μM; Tween 20, 1.62 μM; lysozyme, 19.3 nM). The color code is the same as in the main panel. (b) Value of the observed kinetic constant for adsorption k_{on} as a function of $D^{2/3}/b_m$. The dashed line represents the expected behavior for a constant depletion layer of 20 μm. Inset: Dependence of the measured adsorption rate on the stirring velocity at a fixed concentration of SBSAC in a saline buffer (orange, $C_0 = 3.3\ \mu M$), lysozyme (blue, $C_0 = 71$ nM), and hexane (light green, $C_0 = 55.6\ \mu M$).

the product $\varphi_{eq}\Gamma$. On the other hand, according to Eq. (10), the initial slope of $\varphi(t)$ is always equal to $k_{on}C_0$. Accordingly, we model the rate of adsorption as

$$\Gamma = \frac{k_{on}C_0}{\varphi_{eq}}, \tag{13}$$

where φ_{eq} is given by Eq. (11). In the case of negligible mass limitation, that is, for $N_s/V \ll K_d$, the rates are described by the simple analytical form $\Gamma = k_{on}C_0 + k_{off}$. More generally, the expression of Γ becomes simple for very small and very large values of the analyte concentration C_0 relatively to $C_{1/2}$ and for $C_0 = C_{1/2}$. In these limits, $\Gamma = k_{on}(N_s/V) + k_{off}$, $\Gamma = k_{on}C_0$, and $\Gamma = k_{on}(N_s/V) + 2k_{off}$, respectively. Therefore, the mass-limitation effect tends to increase the observed rate through the term $k_{on}(N_s/V)$. Importantly, for sufficiently large analyte concentrations, the adsorption rate is always given by $k_{on}C_0$, and, therefore, it is not affected by mass limitation. This allows the direct extraction of the apparent kinetic constant for adsorption k_{on} from the slope of the rate $\Gamma(C_0)$ measured for the largest concentrations.

In practice, the data reported in Fig. 5(a) are fitted by using Eq. (13), constraining the values of N_s and $K_d = k_{off}/k_{on}$ to those previously extracted from the study of the equilibrium data (Table II). In this way, only one free parameter (either k_{on} or k_{off}) is determined by the fit. The obtained fitting curves are reported in Fig. 5(a) and its inset, and the values of k_{on} and k_{off} are reported in Table II. As expected from the visual inspection of the behavior of $\Gamma(C_0)$, the desorption kinetic constant k_{off} is rather similar for the three surfactants and the protein, whereas the kinetic constant for adsorption is larger for the protein. Both kinetic constants extrapolated for hexane are much lower than those of the other molecules.

C. Effect of transport limitation

In analogy to the case of ligand-receptor binding, the observed adsorption and desorption process could be affected by the limited transport of analyte molecules from the bulk solution to the sensing surface. This condition occurs when the mixing of molecules in the proximity of the surface is not fast enough in comparison to the intrinsic kinetics for molecular binding, hence leading to smaller values of the measured kinetic rates. An extensive description of transport-limitation phenomena in surface-binding processes is provided in Ref. [57]. Processes characterized by faster binding kinetics, in general, are more affected by such a transport-limitation effect. Importantly, the adsorption kinetics measured in this study are much faster than those typically observed for specific antibody-antigen binding performed with a similar measuring system [10]. Additionally, in the case of adsorption, the transport contribution may play a non-negligible role even for very high flow rates because of the high densities of binding sites on the surface [57]. This is, in fact, an inevitable condition for nonspecific adsorption processes. In the experimental setup employed here, the use of a magnetic stirring bar provides the advantage of a rather efficient mixing of a relatively large volume of solution, approaching the turbulent regime at the highest stirring rates. Nevertheless, extremely large and substantially impractical flow rates or stirring speeds may be required to reduce the effect of transport limitations in the case of large densities of surface-binding sites. Therefore, transport phenomena are expected to play a role in the observed adsorption kinetics. Indeed, an indication of the relevance of the transport limitation is given by the dependence of the observed adsorption kinetics on the stirring speed. As shown in the inset in Fig. 5(b), the measured adsorption rates of hexane are almost insensitive to the rotational speed of the stirrer, whereas those of SBSAC surfactant and lysozyme strongly depend on it. This indicates a more relevant contribution of transport limitation for the surfactants and the protein.

D. Dependence of the observed adsorption kinetics on the molecular size

In the case of kinetics affected by transport limitation, a rather thick layer of fluid in contact with the adsorbing interface experiences a lower concentration of analyte relative to the bulk solution. In this condition, the measured rate is limited by the diffusion time across such a depletion layer. Accordingly, the value of the measured kinetic constants k_{on} and k_{off} are lower than those of the intrinsic kinetic constants $k^i{}_{on}$ and $k^i{}_{off}$, which depend only on the interactions between the analyte molecules and the surface. In particular, considering the effects of transport due to the sample flow and diffusion across the depletion layer, it can be demonstrated (see Appendix B) that the apparent rate k_{on} observed for $C_0 \gg C_{1/2}$ must be in the range $k^{tl}_{on} \leq k_{on} \leq k^i{}_{on}$, where the transport-limited rate k^{tl}_{on} is given by

$$k^{tl}_{on} = F\frac{D^{2/3}}{b_m} \tag{14}$$

and D and b_m are the diffusion coefficient of the molecule and the surface density of adsorption sites, respectively. The parameter F contains all the terms that depend on the cell geometry and flow and not on the properties of the adsorbing molecule. Its value is given by $F = (\dot{\gamma}/L)^{1/3}$, where L is the length of the adsorption area of the sensor along the flow direction and $\dot{\gamma}$ is the derivative of the velocity profile along the surface normal. Similar equations for the transport-limited rate are often encountered in studies concerning sensors in microfluidic cell formats [58,59]. Here we extend the model to the cuvette-based cell and focus on the parameters D and b_m that depend on the specific adsorbing molecule. Figure 5(b) reports the measured values of k_{on} as a function of $D^{2/3}/b_m$. The dashed line indicates the expected scaling for a fully transport-limited case, assuming

a thickness δ of the depletion layer of 20 μm. This represents an upper limit for the value of δ, obtained by assuming that $k_{on} = k_{on}^{tl}$ and that b_m equals the reciprocal of the molecular contact area onto the surface, $1/A_{mol}$. In practice, this is the largest value of δ in agreement with the measured values of k_{on} for all the surfactants and the lysozyme. Indeed, Fig. 5(b) shows that the kinetic rates for adsorption measured for the surfactants and the protein are consistent with the dependence indicated in Eq. (14), whereas hexane does not follow the same scaling. Consequently, the measured kinetics of the surfactants and the protein are consistent with a fully transport-limited regime. Differently, the slower adsorption rates of hexane indicate that transport is not the limiting process in this case, and the observed k_{on} can be ascribed to the molecule-surface interaction.

Remarkably, the scaling indicated by Eq. (14) provides a tool to quantitatively discriminate among the adsorption kinetics of different molecules. In fact, both terms D and b_m scale with the size of the analyte, through either its hydrodynamic radius or the contact area onto the sensing surface, respectively. As reported above, the strength of the adsorption interaction at equilibrium is found to scale with the hydrophobic contact area of the molecule. Here we link the observed transport-limited kinetics to other parameters derived from the molecular size. Overall, the analysis of the adsorption kinetics, in combination with that on the equilibrium discussed in Sec. IV, indicates that the measurement of the spontaneous adsorption on the Hyflon® AD surfaces enables the detection of the presence of different classes of molecules in a solution and the discrimination of them on the basis of their size and hydrophobicity.

VI. CONCLUSIONS

The work presented here provides a threefold advancement in the development of label-free, optical-detection systems based on fluorinated materials index-matched with water: (i) We demonstrate the production of perfluorinated materials in the form of a microporous membrane; (ii) we develop an analytical model to account for the optical response upon adsorption of different index-matched materials, finding a surprisingly simple similarity between the sensitivity of the reflectance- and scattering-based systems; (iii) by means of experimental characterization and modeling of the adsorption of different molecular compounds on a planar surface, we identify the main molecular features affecting the selectivity of the adsorption process.

Remarkably, the adsorption behaviors for different surfactants, a protein, and an oil are very different. In contrast, all the studied surfactants display a similar behavior, despite the different net charges and structures. The molecular size and the molecular area in contact with the surface upon adsorption are identified as relevant parameters, through different specific mechanisms:

(i) the optical response scales with the squared molecular size affecting the thickness of the adsorption layer;
(ii) the strength of the adsorption interaction at equilibrium is found to scale with the molecular hydrophobic contact area on the perfluorinated surface;
(iii) for the fastest adsorption kinetics, where the transport phenomena becomes the limiting effect, the observed adsorption rate scales with the molecular contact area times $D^{2/3}$, where, in general, the diffusion coefficient D scales with the reciprocal molecular size.

These results indicate that, if properly controlled and tuned, the spontaneous adsorption on perfluorinated materials index-matched with water enables the selective detection of different molecular compounds. The selectivity is achieved by considering the amplitudes and kinetics of the optical response, possibly at different dilutions. Accordingly, even molecular classes with a similar refractive index, as in the case of proteins and surfactants, can be identified through the analysis of the adsorption curves. This provides the basis to design a class of optical sensors combining sensitivity, robustness, reusability, and reduced instrumental complexity. These features are constantly sought for different applications and, in particular, for deployable, on-line detection systems for environmental monitoring. As an example, a water basin could be autonomously screened by using the optical-detection method here presented, and, when the response is above a predefined threshold, suitable amounts of sample can be collected and stored for a more specific, lab-based analysis. In this way, the label-free detection based on fluorinated plastics can effectively complement and improve the current analytical approaches for continuous environmental monitoring.

ACKNOWLEDGMENTS

We acknowledge financial support from the European Union Seventh Framework Programme, through the NAPES project (Grant Agreement No. 604241).

APPENDIX A: PRODUCTION OF MICROPOROUS MEMBRANES

The membranes of Hyflon® AD40 (Solvay Specialty Polymers, Italy) are realized by the nonsolvent induced phase separation method [60]. We dissolve 7.5 g of the perfluorinated polymer into 30 mL of methoxyperfluorobutane, HFE 7100 (3M-Novec) and 2.5 g of cyclohexanone (Sigma-Aldrich). This solution is used to realize a 250-μm film by casting on a glass plate cooled with dry ice. The plate is then immediately placed into a coagulation bath composed by a 1:1 mixture of acetone and ethanol for 10 min. Then, the plate is immersed in a bath of ethanol for another 10 min to extract the residual solvent. We store the samples in a 30%–70% mixture of ethanol and water. We obtain membranes with a thickness of 80–100 μm and a porosity of 60%–70%. The thermogravimetric analysis

reveals only 1% wt of residual solvent in the membranes. The cross-section SEM image [Fig. 1(b)] was taken after breaking the sample in liquid nitrogen, without any kind of metallization. Before the optical measurements, we wash the membrane with MilliQ water several times and then we soak it for 15 h with water. Finally, we degas the sample for 10 min to remove the air bubbles.

The refractive index of the membrane is obtained as the extrapolated minimum of scattered light as a function of the refractive index of the solvent. The membranes are soaked in different mixtures of water and ethanol, whose refractive index is measured by an Abbe refractometer. The measurements give a membrane refractive index of $n = 1.3309 \pm 0.0002$.

APPENDIX B: TRANSPORT-LIMITED ADSORPTION KINETICS

In general, binding or adsorption processes are characterized by intrinsic kinetic constants $k^i_{\rm on}$ and $k^i_{\rm off}$ that depend on the interactions between the analyte molecules and the surface. Only in the case of fast enough transport of molecules (i.e., fast flow and mixing near the surface), $k^i_{\rm on}$ and $k^i_{\rm off}$ are equal to the observed kinetic constants $k_{\rm on}$ and $k_{\rm off}$, respectively. More generally, the transport process may somewhat affect both the observed kinetic constants $k_{\rm on}$ and $k_{\rm off}$ in the same way. The condition of transport limitation involves the presence of a layer of fluid on the surface with a transiently lower concentration of analyte relative to the bulk solution. The measured rate is affected by the diffusion across such a depletion layer. The thickness δ of the depletion zone depends on the flux close to the surface, on the geometry of the measuring cell, and on the free diffusion of the studied molecule. The value of δ can be estimated as [57]

$$\delta = \sqrt[3]{\frac{LD}{\dot\gamma}}, \tag{B1}$$

where L is the length of the adsorption area of the sensor along the flow direction, $\dot\gamma$ is the derivative of the velocity profile along the surface normal, and D is the diffusion coefficient of the molecule. In general, transport limitation is more relevant for larger values of δ. However, according to Eq. (B1), δ scales only with the cube root of the flow parameter $\dot\gamma$.

A common approach to compute the effect of transport on the observable kinetic rates is to consider two regions (i.e., two compartments) with different concentrations of analyte: the depletion layer and the rest of the sample volume. The two compartments have two spatially uniform concentrations: $C_d(t)$ and $C_{\rm bulk}(t)$, respectively [61]. Using this approximation, the adsorption process is still modeled by Eq. (10) with the substitution $C_0 = C_d$ and with the value of C_d provided by the diffusive equilibrium between the two compartments. Considering an initial condition without analyte molecules in a cuvette and a sudden increase of the concentration from zero to $C_{\rm bulk}$, for a negligible value of δ the initial flux of molecules toward the surface is given by $J^{\rm kin} = k^i_{\rm on} C_{\rm bulk} b_m$, where b_m represents the surface density of the available binding sites. At the other extreme, a purely diffusive flux across the depletion layer is given by $J^{\rm diff} = DC_{\rm bulk}/\delta$, according to Fick's first law of diffusion. The ratio $Da = J^{\rm kin}/J^{\rm diff}$ is known as the Damköhler number, and its value indicates to what extent the observed kinetics is affected by transport limitation [57,58]. The measured characteristic time $\tau_{\rm obs} = 1/\Gamma$ for a binding process on a surface differs from the intrinsic molecular interaction time $\tau_R = (k^i_{\rm on} C_0 + k^i_{\rm off})^{-1}$ according to

$$\tau_{\rm obs} = (1 + Da)\tau_R. \tag{B2}$$

In the case of pronounced transport limitation ($Da \gg 1$) and for $C_0 \gg C_{1/2}$, from the above definition of Da we derive that $\Gamma = k^{tl}_{\rm on} C_0$, where

$$k^{tl}_{\rm on} = \frac{D}{\delta b_m} \tag{B3}$$

represents the transport-limited rate for adsorption. Accordingly, the value of the apparent kinetic constant for binding $k_{\rm on}$ must be in the range $k^{tl}_{\rm on} \le k_{\rm on} \le k^i_{\rm on}$.

In order to investigate the dependence of the observed adsorption kinetics on the molecular properties, we focus on the limiting case of a fully transport-limited process. Substituting the expression of δ given in Eq. (B1) into Eq. (B3), the terms that depend on the cell geometry and flow and not on the properties of the molecular analyte are grouped in the parameter $F = (\dot\gamma/L)^{1/3}$, thus leading to Eq. (14).

[1] B. Zhmud and F. Tiberg, Interfacial dynamics and structure of surfactant layers, Adv. Colloid Interface Sci. **113**, 21 (2005).

[2] F. Zaera, Probing liquid/solid interfaces at the molecular level, Chem. Rev. **112**, 2920 (2012).

[3] B. Stuart, in *Kirk-Othmer Encyclopedia of Chemical Technology* (Wiley, Hoboken, NJ, 2005).

[4] P. Patnaik, *Handbook of Environmental Analysis: Chemical Pollutants in Air, Water, Soil, and Solid Wastes*, 2nd ed. (CRC Press, Boca Raton, FL, 2010).

[5] S. González, D. Barceló, and M. Petrovic, Advanced liquid chromatography-mass spectrometry (LC-MS) methods applied to wastewater removal and the fate of surfactants in the environment, TrAC, Trends in Analytical Chemistry **26**, 116 (2007).

[6] T. Reemtsma, Liquid chromatography-mass spectrometry and strategies for trace-level analysis of polar organic pollutants, J. Chromatogr. A **1000**, 477 (2003).

[7] M. Shim, N. W. S. Kam, R. J. Chen, Y. Li, and H. Dai, Functionalization of carbon nanotubes for biocompatibility and biomolecular recognition, Nano Lett. **2**, 285 (2002).

[8] S. Wu, Q. He, C. Tan, Y. Wang, and H. Zhang, Graphene-based electrochemical sensors, Small **9**, 1160 (2013).

[9] B. R. Baker, R. Y. Lai, M. S. Wood, E. H. Doctor, A. J. Heeger, and K. W. Plaxco, An electronic, aptamer-based small-molecule sensor for the rapid, label-free detection of cocaine in adulterated samples and biological fluids, J. Am. Chem. Soc. **128**, 3138 (2006).

[10] F. Giavazzi *et al.*, Multispot, label-free biodetection at a phantom plastic-water interface, Proc. Natl. Acad. Sci. U.S.A. **110**, 9350 (2013).

[11] F. Giavazzi *et al.*, A fast and simple label-free immunoassay based on a smartphone, Biosens. Bioelectron. **58**, 395 (2014).

[12] R. Lanfranco and M. Buscaglia, *Reference Module in Materials Science and Materials Engineering* (Elsevier, Oxford, 2016), pp. 1–10.

[13] D. Prosperi, C. Morasso, F. Mantegazza, M. Buscaglia, L. Hough, and T. Bellini, Phantom nanoparticles as probes of biomolecular interactions, Small **2**, 1060 (2006).

[14] C. Morasso, M. Colombo, S. Ronchi, L. Polito, S. Mazzucchelli, D. Monti, M. Buscaglia, T. Bellini, and D. Prosperi, Towards a universal method for the stable and clean functionalization of inert perfluoropolymer nanoparticles: Exploiting photopolymerizable amphiphilic diacetylenes, Adv. Funct. Mater. **20**, 3932 (2010).

[15] A. Ghetta, D. Prosperi, F. Mantegazza, L. Panza, S. Riva, and T. Bellini, Light scattered by model phantom bacteria reveals molecular interactions at their surface, Proc. Natl. Acad. Sci. U.S.A. **102**, 15866 (2005).

[16] M. Salina, F. Giavazzi, E. Ceccarello, F. Damin, M. Chiari, M. Ciuffo, G. P. Accotto, and M. Buscaglia, Multi-spot, label-free detection of viral infection in complex media by a non-reflecting surface, Sens. Actuators, B **223**, 957 (2016).

[17] W. H. Tuminello, Solubility of Poly(Tetrafluoroethylene) and its Copolymers, in *Fluoropolymers 2*, edited by G. Hougham *et al.* (Kluwer Academic, Boston, 1999).

[18] B. Jones, Fluoropolymers for coating applications, JCT CoatingsTech **5**, 44 (2008).

[19] E. Giannetti, Semi-crystalline fluorinated polymers, Polym. Int. **50**, 10 (2001).

[20] T. Bellini, V. Degiorgio, F. Mantegazza, F. A. Marsan, and C. Scarnecchia, Electrokinetic properties of colloids of variable charge. I. Electrophoretic and electro-optic characterization, J. Chem. Phys. **103**, 8228 (1995).

[21] F. Mantegazza, T. Bellini, M. Buscaglia, V. Degiorgio, and D. A. Saville, Electrokinetic properties of colloids of variable charge. III. Observation of a Maxwell-Wagner relaxation mechanism by high-frequency electric-birefringence spectroscopy, J. Chem. Phys. **113**, 6984 (2000).

[22] M. Rabe, D. Verdes, and S. Seeger, Understanding protein adsorption phenomena at solid surfaces, Adv. Colloid Interface Sci. **162**, 87 (2011).

[23] R. Atkin, V. S. J. Craig, E. J. Wanless, and S. Biggs, Mechanism of cationic surfactant adsorption at the solid-aqueous interface, Adv. Colloid Interface Sci. **103**, 219 (2003).

[24] J. L. Wolgemuth, R. K. Workman, and S. Manne, Surfactant aggregates at a flat, isotropic hydrophobic surface, Langmuir **16**, 3077 (2000).

[25] S. Paria and K. C. Khilar, A review on experimental studies of surfactant adsorption at the hydrophilic solid-water interface, Adv. Colloid Interface Sci. **110**, 75 (2004).

[26] S. O. Nielsen, G. Srinivas, C. F. Lopez, and M. L. Klein, Modeling Surfactant Adsorption on Hydrophobic Surfaces, Phys. Rev. Lett. **94**, 228301 (2005).

[27] X. López-Lozano, L. A. Pérez, and I. L. Garzón, Enantiospecific Adsorption of Chiral Molecules on Chiral Gold Clusters, Phys. Rev. Lett. **97**, 233401 (2006).

[28] C. Brumaru and M. L. Geng, Interaction of surfactants with hydrophobic surfaces in nanopores, Langmuir **26**, 19091 (2010).

[29] E. Finot, A. Fabre, A. Passian, and T. Thundat, Dynamic and Static Manifestation of Molecular Absorption in Thin Films Probed by a Microcantilever, Phys. Rev. Applied **1**, 024001 (2014).

[30] D. Lohse and X. Zhang, Surface nanobubbles and nanodroplets, Rev. Mod. Phys. **87**, 981 (2015).

[31] C. Toccafondi, M. Prato, G. Maidecchi, A. Penco, F. Bisio, O. Cavalleri, and M. Canepa, Optical properties of Yeast Cytochrome c monolayer on gold: An in situ spectroscopic ellipsometry investigation, J. Colloid Interface Sci. **364**, 125 (2011).

[32] I. Solano, P. Parisse, F. Gramazio, O. Cavalleri, G. Bracco, M. Castronovo, L. Casalis, and M. Canepa, Spectroscopic ellipsometry meets AFM nanolithography: About hydration of bio-inert oligo(ethylene glycol)-terminated self assembled monolayers on gold, Phys. Chem. Chem. Phys. **17**, 28774 (2015).

[33] F. L. Pedrotti, L. M. Pedrotti, and L. S. Pedrotti, *Introduction to Optics, 3/E*, 3rd ed. (Addison-Wesley, Reading, MA, 2006).

[34] V. Arcella, A. Ghielmi, and G. Tommasi, High performance perfluoropolymer films and membranes, Ann. N.Y. Acad. Sci. **984**, 226 (2003).

[35] P. Wiltzius, F. S. Bates, S. B. Dierker, and G. D. Wignall, Structure of porous vycor glass, Phys. Rev. A **36**, 2991 (1987).

[36] L. Cipelletti, M. Carpineti, and M. Giglio, Fractal morphology, spatial order, and pore structure in microporous membrane filters, Langmuir **12**, 6446 (1996).

[37] H. C. van de Hulst, *Light Scattering by Small Particles* (Dover, New York, 1957).

[38] R. Piazza and V. Degiorgio, Light scattering study of spherical latex particles: Measurement of surfactant adsorption and of intrinsic anisotropy, Opt. Commun. **92**, 45 (1992).

[39] P. Atkins and J. de Paula, *Atkins' Physical Chemistry*, 9th ed. (Oxford University, New York, 2010).

[40] B. Esteban Fernández de Ávila, H. M. Watkins, J. M. Pingarrón, K. W. Plaxco, G. Palleschi, and F. Ricci, Determinants of the detection limit and specificity of surface-based biosensors, Anal. Chem. **85**, 6593 (2013).

[41] E. Iritani, S. Tachi, and T. Murase, Influence of protein adsorption on flow resistance of microfiltration membrane, Colloids Surf. A **89**, 15 (1994).

[42] J. Vörös, The density, and refractive index of adsorbing protein layers, Biophys. J. **87**, 553 (2004).

[43] R. M. Weinheimer, D. F. Evans, and E. Cussler, Diffusion in surfactant solutions, J. Colloid Interface Sci. **80**, 357 (1981).

[44] H. C. Gao, R. X. Zhu, X. Y. Yang, S. Z. Mao, S. Zhao, J. Y. Yu, and Y. R. Du, Properties of polyethylene glycol (23) lauryl ether with cetyltrimethylammonium bromide in mixed aqueous solutions studied by self-diffusion coefficient NMR, J. Colloid Interface Sci. **273**, 626 (2004).

[45] D. Brune and S. Kim, Predicting protein diffusion coefficients, Proc. Natl. Acad. Sci. U.S.A. **90**, 3835 (1993).

[46] C. R. Wilke and P. Chang, Correlation of diffusion coefficients in dilute solutions, AIChE J. **1**, 264 (1955).

[47] J. T. K. Milton and J. Rosen, *Surfactants and Interfacial Phenomena*, 4th ed. (Wiley, New York, 2012).

[48] N. G. Gaylord and J. H. Gibbs, in *Physical Chemistry of Macromolecules*, edited by C. Tanford (Wiley, New York, 1962).

[49] S. F. Turner, S. M. Clarke, A. R. Rennie, P. N. Thirtle, D. J. Cooke, Z. X. Li, and R. K. Thomas, Adsorption of sodium dodecyl sulfate to a polystyrene/water interface studied by neutron reflection and attenuated total reflection infrared spectroscopy, Langmuir **15**, 1017 (1999).

[50] R. Atkin, V. S. J. Craig, and S. Biggs, Adsorption kinetics and structural arrangements of cationic surfactants on silica surfaces, Langmuir **16**, 9374 (2000).

[51] A. J. Ricco, G. C. Frye, and S. J. Martin, Determination of BET surface areas of porous thin films using surface acoustic wave devices, Langmuir **5**, 273 (1989).

[52] G. B. Sigal, M. Mrksich, and G. M. Whitesides, Effect of surface wettability on the adsorption of proteins and detergents, J. Am. Chem. Soc. **120**, 3464 (1998).

[53] W. C. Wimley and S. H. White, Experimentally determined hydrophobicity scale for proteins at membrane interfaces, Nat. Struct. Biol. **3**, 842 (1996).

[54] K. D. Danov and P. A. Kralchevsky, The standard free energy of surfactant adsorption at air/water and oil/water interfaces: Theoretical vs. empirical approaches, Colloid J. **74**, 172 (2012).

[55] S. H. Chen and C. W. Frank, Infrared and fluorescence spectroscopic studies of self-assembled n-alkanoic acid monolayers, Langmuir **5**, 978 (1989).

[56] A. A. Levchenko, B. P. Argo, R. Vidu, R. V. Talroze, and P. Stroeve, Kinetics of sodium dodecyl sulfate adsorption on and desorption from self-assembled monolayers measured by surface plasmon resonance, Langmuir **18**, 8464 (2002).

[57] T. M. Squires, R. J. Messinger, and S. R. Manalis, Making it stick: Convection, reaction and diffusion in surface-based biosensors, Nat. Biotechnol. **26**, 417 (2008).

[58] R. Hansen, H. Bruus, T. H. Callisen, and O. Hassager, Transient convection, diffusion, and adsorption in surface-based biosensors, Langmuir **28**, 7557 (2012).

[59] P. Schuck, Kinetics of ligand binding to receptor immobilized in a polymer matrix, as detected with an evanescent wave biosensor. I. A computer simulation of the influence of mass transport, Biophys. J. **70**, 1230 (1996).

[60] R. W. Baker, *Membrane Technology and Applications*, 3rd ed. (Wiley, New York, 2012).

[61] D. G. Myszka, X. He, M. Dembo, T. A. Morton, and B. Goldstein, Extending the range of rate constants available from BIACORE: Interpreting mass transport-influenced binding data, Biophys. J. **75**, 583 (1998).